

# Visualizing Topology of Real-Energy Gapless Phase Arising from Exceptional Point

X. M. Yang, P. Wang, L. Jin,\* and Z. Song†  
*School of Physics, Nankai University, Tianjin 300071, China*

The discovery of novel topological phase advances our knowledge of nature and stimulates the development of applications. In non-Hermitian topological systems, the topology of band touching exceptional points is very important. Here we propose a real-energy topological gapless phase arising from exceptional points in one dimension, which has identical topological invariants as the topological gapless phase arising from degeneracy points. We develop a graphic approach to characterize the topological phases, where the eigenstates of energy bands are mapped to the graphs on a torus. The topologies of different phases are visualized and distinguishable; and the topological gapless edge state with amplification appropriate for topological lasing exists in the nontrivial phase. These results are elucidated through a non-Hermitian Su-Schrieffer-Heeger ladder. Our findings open new way for identifying topology phase of matter from visualizing the eigenstates.

*Introduction.*—Topological phase of matter has become a frontier research field due to their novel features for potential applications [1–20]. Majorana [21–24], Dirac [25–30], and Weyl fermions [31–35] predicted in high-energy physics are discovered in this fertile ground. These concepts stimulate an interesting topic of topological gapless phases/semimetals [36–44]. The symmetry protected nodal points in topological gapless phase are topological defects of an auxiliary vector field and are irremovable until they meet and annihilates in pairs. The topology of gapless bands can be characterized by kink in one-dimension (1D) [45] or vortex of skyrmion in two-dimension (2D) [41, 42].

Nowadays, the great efforts have been made to unravel the mystery of non-Hermitian physics [46–61]. Non-Hermitian phase transition occurs at exceptional point (EP) [52–55], which is a unique concept in non-Hermitian systems and has exotic topology related to Riemann surface [62–77]. The investigations of topological physics have been extended to non-Hermitian region [78–107]. The non-Hermitian topological systems under various combined symmetries including the parity-time ( $\mathcal{PT}$ ) symmetry are investigated [108–116]. The non-Hermitian topological invariant and band theory are established [117–119]. The  $\mathcal{PT}$ -symmetric interface states are realized in passive optical systems [120–122]. Furthermore, the edge state lasing is demonstrated in active optical systems [123–128]. The high-order non-Hermitian topological systems [129–133], the breakdown of bulk-boundary correspondence [134–142], and the topological classifications [142–146] are studied.

In non-Hermitian topological systems, the gap closing in energy band is usually associated with EPs instead of degenerate points (DPs) [117–119, 147, 148]. The band touching EP pairs split from single DPs are connected by open Fermi arcs [148–151]; alternatively, non-Hermitian semimetals exhibit nodal phases with symmetry protected EPs rings and surfaces [152–158]; the corresponding energy bands in the non-Hermitian gapless phases are all complex. The complex-energy bands associated EPs are systematically studied [146] and they

are dramatically different from the gapless phase in a Hermitian system. In contrast to the Hermitian topological gapless phase, a non-Hermitian topological gapless phase is typically characterized by two types of winding numbers; an additional winding number solely for non-Hermitian systems is defined to characterize the topology of Riemann sheet energy bands [118, 119, 142]. The real-energy energy band does not exponentially decay or increase as time and has a zero winding in contrast to the complex energy band. Thus, two winding numbers are insufficient to distinguish the gapless phases arising from EPs and DPs.

The aim of this Letter is to propose a real-energy gapless phase associated with band touching EPs. The balanced gain and loss are introduced in chiral symmetric Hermitian topological insulators to create the gapless phase arising from EPs, where robust zero modes with amplification and attenuation are generated for nontrivial topology. We offer a powerful graphic approach to visualize the topological features of different phases. The rich topological phases of either gapped (separable) or gapless, either Hermitian or non-Hermitian band touching, and either trivial or nontrivial phases are all distinguishable from the geometrical topologies of eigenstate graphs. The essence of eigenstate graphs dramatically differs from the knotted or linked nodal lines in semimetals that representing the zero-energy (equal-energy) surface [154, 155, 159]. In the graphic approach, the graphic eigenstates of real gapless bands arising from EPs form a network; the topological nature of which is characterized by its nodes, branches, and independent loops. The networks with different links, fixed/movable nodes correspond to different topological phases; other gapless and gapped phases possess distinct geometric graphs.

*Gapless phase arising from EPs.*—In the theory for topological insulators [1, 2], the energy band is insufficient to determine the full topological character of a phase of matter. The bulk topological features are encoded in the eigenstates. We consider a prototype of non-Hermitian topological system: the 1D two-band model. In the momentum space, the core matrix reads  $h_k = \mathbf{B} \cdot \sigma$ ,

where  $\mathbf{B} = (B_x, B_y, B_z)$  is an effective magnetic field, and  $\sigma = (\sigma_x, \sigma_y, \sigma_z)$  is the Pauli matrix;  $B_x$  and  $B_y$  are real, but  $B_z$  is imaginary. The energy bands are tighten under the influence of  $B_z$ ; however, the topological phase transition in  $h_k$  is not affected by  $B_z$ . Thus, the gapless phase is created via increasing  $B_z$  in the gapped phase till a non-Hermitian phase transition.

*Graphic eigenstate.*—For  $B^2 = B_x^2 + B_y^2 + B_z^2 \geq 0$ , the eigen values  $\varepsilon_k^\pm = \pm B$  are real with corresponding eigenstates

$$|\psi_k^\pm\rangle = \frac{1}{\sqrt{2}} \begin{pmatrix} e^{i\varphi_\pm(k)} \\ 1 \end{pmatrix}, \quad (1)$$

where  $\varphi_+(k) = \arctan(-B_y/B_x) + \arctan(-iB_z/B)$  and  $\varphi_-(k) = \arctan(-B_y/B_x) \pm \pi - \arctan(-iB_z/B)$  are real functions with a period  $2\pi$ . The varying directions of  $\varphi_\pm(k)$  and  $\mathbf{B}$  are the same. Therefore,  $\varphi_\pm(k)$  as the kernel of eigenstates  $|\psi_k^\pm\rangle$  provides the information of the topological nature of  $h_k$ . Notably,  $|\psi_k^\pm\rangle$  can be represented by a loop on the torus spanned by  $\varphi_\pm(k)$  and  $k$ , referred to as the graphic eigenstates.

In the  $k$  space,  $h_k$  is  $\mathcal{PT}$ -symmetric  $(\mathcal{PT})^{-1} h_k (\mathcal{PT}) = h_k$  and  $\mathcal{CT}$ -symmetric  $(\mathcal{CT})^{-1} h_k (\mathcal{CT}) = -h_{-k}$ , where the operators  $\mathcal{PT} = \sigma_x \mathcal{K}$ ,  $\mathcal{CT} = \sigma_z \mathcal{K}$ , and  $\mathcal{K}$  is the complex conjugation. The  $\mathcal{PT}$  symmetry is related to the reality of the spectrum; while the  $\mathcal{CT}$  symmetry protects the system topology. For an arbitrary eigenstate  $|\psi_k^\pm\rangle$ , the  $\mathcal{CT}$  symmetry requires another eigenstate satisfying  $|\psi_{-k}^\pm\rangle = \mathcal{CT} |\psi_k^\pm\rangle$ , which leads to

$$\varphi_+(k) + \varphi_-(-k) = \pm\pi. \quad (2)$$

In particular, when the EP appears at  $k_c$ , two eigenstates  $|\psi_{k_c}^+\rangle$  and  $|\psi_{k_c}^-\rangle$  coalesce to one denoted as  $|\psi_{k_c}^0\rangle$ . The  $\mathcal{CT}$  symmetry ensures  $|\psi_{-k_c}^0\rangle = \mathcal{CT} |\psi_{k_c}^0\rangle$ , i.e., the existence of a pair of EPs with zero energy for  $k_c \neq 0, \pi$ ; any EP cannot be separately removed, but the EP position changes as the system parameters. When  $k_c = 0, \pi$ , we have one fixed EP with  $\varphi_\pm(k_c) = \pi/2$  or  $-\pi/2$ .

For a Hermitian system with  $B_z = 0$ , we always have  $\varphi_-(k) = \varphi_+(k) \pm \pi$ . In the presence of a DP, two energy bands usually form a single knot [Fig. 4(c)]. In the absence of DPs,  $\mathbf{B} \neq \mathbf{0}$ , two energy bands form two loops without intersection; this is similar as the gapped non-Hermitian phase shown in Figs. 4(a) and 4(b). For a non-Hermitian system, the effective magnetic field  $\mathbf{B}$  is complex. In contrast to two eigenstates of a Hermitian matrix that represented by two opposite points on the torus due to the orthogonality, two eigenstates of the real-energy bands in a non-Hermitian matrix represented by two points can have arbitrary positions on the torus; and they meet when eigenstates coalesce at the EPs, where  $\varphi_-(k) = \varphi_+(k)$ . Then, two graphic eigenstates constitute a network [Figs. 4(e)-1(h)]. The network on the  $\varphi$ - $k$  torus provides a complete topological picture for the real-energy gapless phase arising from EPs, the topological

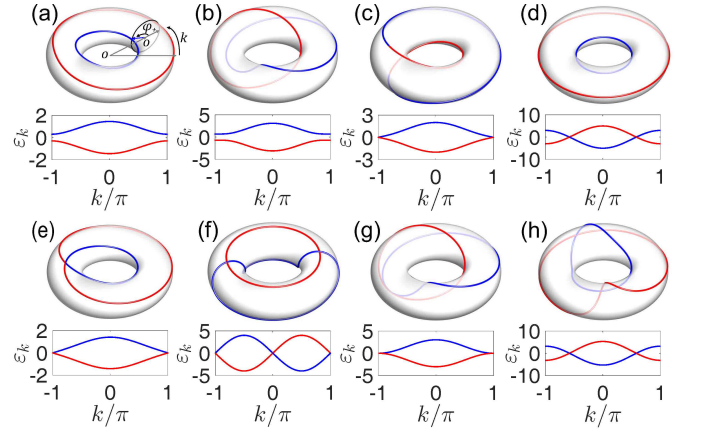


FIG. 1. Graphic eigenstates and energy bands of the SSH ladder.  $t = 1$  and  $(v, w, \gamma)$  is (a)  $(1/4, 1/4, 2/5)$ , (b)  $(2, 2/7, 1)$ , (c)  $(1/4, 3/4, 0)$ , (d)  $(2, 2, 0)$ , (e)  $(1/4, 1/4, \gamma_c)$ , (f)  $(-2, 2, \gamma_c)$ , (g)  $(2, 2/7, \gamma_c)$ , and (h)  $(3, 3/2, \gamma_c)$ .  $\gamma_c$  is chosen Eq. (9) in (e) and (f); but chosen Eq. (8) in (g) and (h). (c) and (d) are the Hermitian case; in the non-Hermitian case, (a), (e), and (f) [(b), (g), and (h)] are in the topologically trivial (nontrivial) phase. The gapless phases arising from EPs are (e)-(h).

features of which are reflected from the network topology. Notably, the graphs represent the eigenstate rather than the zero energy, which essentially differs from the EP links or knotted nodal lines of EPs [138, 139, 152–159].

*Topological characterization.*—In general cases, multiple EPs may appear; accordingly, the graphic eigenstates may form complicate networks. The geometrical topology of any network satisfies a fundamental fact: the numbers of nodes  $n$ , independent loops  $l$ , and branches  $b$  fulfill

$$n = b - l + 1. \quad (3)$$

An independent loop must contain at least one branch that not belongs to any other loop. For instance, we have  $n = 1$  (2),  $b = 2$  (4),  $l = 2$  (3) for the network shown in Fig. 4(g) [Fig. 4(h)]. This graphic approach is especially helpful in characterizing the real-energy topological gapless phase arising from EPs.

Two graphic eigenstate loops are unlinked [Fig. 4(a)] or linked [Fig. 4(b)], which indicate the trivial or nontrivial topology. To verify this assertion, we point out that the varying direction of  $\varphi_\pm(k)$  accumulated in a period of  $k$  defines a winding number

$$\mathcal{N}_\pm = (2\pi)^{-1} \int_0^{2\pi} \nabla_k \varphi_\pm(k) dk. \quad (4)$$

Besides, the average values of Pauli matrices under two eigenstates  $|\psi_k^\pm\rangle$  yield  $\langle \sigma_x \rangle_\pm = \cos[-\varphi_\pm(k)]$ ,  $\langle \sigma_y \rangle_\pm = \sin[-\varphi_\pm(k)]$ , and  $\langle \sigma_z \rangle_\pm = 0$  [160]; which define a planar vector field that associated with the upper ( $|\psi_k^+\rangle$ ) or lower ( $|\psi_k^-\rangle$ ) band

$$\mathbf{F}_\pm(k) = (\langle \sigma_x \rangle_\pm, \langle \sigma_y \rangle_\pm). \quad (5)$$

$\mathbf{F}_{\pm}(k)$  characterizes the topological properties of energy band [41, 42, 137, 149]. The winding number associated with  $\mathbf{F}_{\pm}(k)$  is  $(2\pi)^{-1} \int_0^{2\pi} \nabla_k \arg \mathbf{F}_{\pm}(k) dk$ , which equals to the winding number  $\mathcal{N}_{\pm}$ . The coincidence of varying directions of  $\varphi_{\pm}(k)$  and  $\mathbf{F}_{\pm}(k)$  indicates that the topological properties of energy band are reflected from the kernel of eigenstate  $\varphi_{\pm}(k)$ .  $2\pi\mathcal{N}_{\pm}$  is the nonzero rotation angle of  $\varphi_{\pm}(k)$  accumulated in a period of  $k$ , indicating the nontrivial topology of the gapped or gapless phase, and the graphic eigenstate loops are linked. Notably, the winding numbers for the two bands are identical  $\mathcal{N} \equiv \mathcal{N}_+ = \mathcal{N}_-$ .

For the gapless phase with EPs, the topology of EPs arising from entirely real-energy bands are in a striking difference from the EPs in the complex energy bands. The difference is revealed from another winding number  $\mathcal{W}_{\text{EP}} = (2\pi)^{-1} \int_{-\pi}^{\pi} \nabla_k \arg E_+(k) dk$  that characterizing the Riemann sheets [118, 119, 142]. Notably,  $\mathcal{W}_{\text{EP(DP)}} = 0$  for the EPs (DPs) of real-energy gapless bands in contrast to  $\mathcal{W}_{\text{EP}} = \pm 1/2$  for the EPs in the complex energy bands [99, 118, 148]. However, the topologies of real-energy gapless phases arising from DPs and EPs dramatically differ from each other; the node (network configuration) is absent for the gapless bands with DPs, while the presence of node is a typical feature for the gapless bands with EPs.

*Non-Hermitian SSH ladder.*—As a prototype of one-dimensional non-Hermitian topological system, the  $\mathcal{PT}$ -symmetric non-Hermitian Su-Schrieffer-Heeger (SSH) model is experimentally realized in the coupled waveguides [82, 121, 122], coupled resonators [120], and polariton micropillars [123]. The essential features of the  $\mathcal{PT}$ -symmetric non-Hermitian system are captured even though the system is passive; the active non-Hermitian SSH model is realized with additional pumping [123–125]. Candidates for the experimental realization of non-Hermitian topological systems include photonic crystals [5, 9, 161], ultracold atomic gasses [8, 79], acoustic lattices [162–164], and electric circuits [130, 165–167]. We employ a non-Hermitian SSH ladder [Fig. 2(a)] to elucidate our findings. Introducing additional loss  $-2i\gamma$  in one sublattice (the pink lattice) generates a passive non-Hermitian SSH ladder [52]; an overall decay rate  $-i\gamma$  offset in both sublattices yields a  $\mathcal{PT}$ -symmetric non-Hermitian SSH ladder [108]; alternatively, we can consider an active  $\mathcal{PT}$ -symmetric non-Hermitian SSH ladder constituted by two coupled SSH chains incorporated gain and loss [124]. The Hamiltonian in the real space reads

$$H = \sum_{j=1}^N (wa_{j+1}^\dagger b_j + va_j^\dagger b_{j+1} + ta_j^\dagger b_j + \text{H.c.}) + i\gamma(a_j^\dagger a_j - b_j^\dagger b_j), \quad (6)$$

where  $a_j^\dagger$  ( $b_j^\dagger$ ) is the creation operator of the  $j$ th site in the sublattice  $A$  ( $B$ ).  $H$  is a two-leg ladder with  $2N$  sites, each leg is a  $\mathcal{PT}$ -symmetric SSH chain with stag-

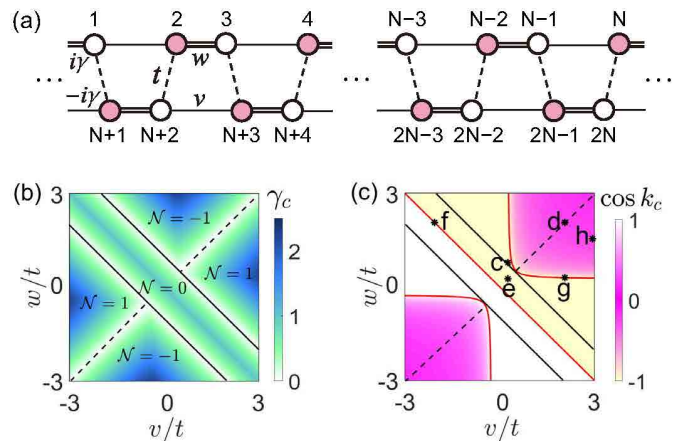


FIG. 2. (a) Schematic of the non-Hermitian SSH ladder. The gain (loss) is in sublattice  $A$  ( $B$ ) in white (pink). (b) Phase diagram and critical  $\gamma_c$  [Eqs. (8) and (9)]. (c)  $\cos(k_c)$  for the EPs. Red solid curves divide the  $v$ - $w$  plane into four regions; the band gap closes at EPs at  $k_c, 0$  and  $\pi$ . Two hyperbola curves are  $|w + v| = 4wv/t$ . Stars  $c$  to  $f$  are marked for the cases in Fig. 4.

gered real couplings  $w$  and  $v$  [120–125]; two ladder legs are coupled at the strength  $t$  after one leg glided by one site.  $H$  is a simple generalization of the  $\mathcal{PT}$ -symmetric non-Hermitian SSH model. Applying the Fourier transformation, the Hamiltonian under periodical boundary condition is rewritten as  $H = \sum_k h_k = \sum_k \mathbf{B} \cdot \boldsymbol{\sigma}$ . The core matrix reads

$$h_k = \begin{pmatrix} i\gamma & we^{ik} + ve^{-ik} + t \\ we^{-ik} + ve^{ik} + t & -i\gamma \end{pmatrix}. \quad (7)$$

The non-Hermitian SSH ladder has  $\mathcal{PT}$  symmetry and chiral-time ( $\mathcal{CT}$ ) symmetry [81, 108, 110]. The corresponding energy bands  $\varepsilon_k^{\pm}$  for the graphic eigenstates are depicted as a function of  $k$  in the lower panel of Fig. 4.

In the gapped phase, the graphic eigenstates are two separated loops on the  $\varphi$ - $k$  torus. The two loops are unlinked [Fig. 4(a)] in the topologically trivial phase with  $\mathcal{N} = 0$ ; and are linked [Fig. 4(b)] in the topologically nontrivial phase with  $\mathcal{N} = \pm 1$ . The system has the gapless phase arising from DPs in the Hermitian case; at  $w + v = \pm t$ , we notice one fixed DP [black solid line in Fig. 2(b)], and two movable DPs at  $w = v$  [black dashed line in Fig. 2(b)] in region  $|w + v| > t$  that characterized by the vector field kinks [45]. One fixed DP appears at  $k_c = 0$  or  $\pi$ . The energy bands constitute a single band and the graphic eigenstates form a knot [Fig. 4(c)]. At  $w = v$ , two components of the magnetic field  $\mathbf{B}$  vanish, the band gap closes and two movable DPs appear at  $\cos k_c = -t/(2v)$ . Two loops on the  $\varphi$ - $k$  torus are separated without any intersection [Fig. 4(d)].

As gain and loss increase, the band gap shrinks and closes at the critical non-Hermiticity

$$\gamma_c = |v - w| \sqrt{1 - t^2/(4vw)}, \quad (8)$$

in the region  $|w + v| \leq 4wv/t$ , where the EPs are movable in the momentum space and appear at  $\cos k_c = -t(w + v)/(4wv)$ ; otherwise, the band gap closes at the critical non-Hermiticity

$$\gamma_c = |w + v \pm t|, \quad (9)$$

and the EPs are fixed in the momentum space and appear at  $k_c = 0$  or  $\pi$ .  $\gamma_c$  for the band gap closing is depicted in Fig. 2(b);  $\cos k_c$  for the location of EPs are depicted in Fig. 2(c). In Fig. 2(b), the black dashed line separates two phases with winding numbers  $\mathcal{N} = 1$  and  $\mathcal{N} = -1$ ; while the black solid line separates phases with winding numbers  $\mathcal{N} = \pm 1$  and  $\mathcal{N} = 0$ .

The hyperbola  $|w + v| = 4wv/t$  and line  $w + v = 0$  divide the  $w$ - $v$  plane into four real-energy gapless phases with distinct topological characters [Fig. 2(c)]. The topological feature is clearly revealed by the graphic approach: (i) For  $\gamma < \gamma_c$ , two real-energy bands are separated without any EP; two loops on the  $\varphi$ - $k$  torus have none intersection [Figs. 4(a) and (b)]. (ii) For  $\gamma = \gamma_c$  in the region  $|w + v| < 4wv/t$  except for  $w = v$ , two loops on the  $\varphi$ - $k$  torus have two robust nodes [Fig. 4(h)], which are movable but irremovable as the system parameters  $w$  and  $v$ ; two movable nodes merge to a single fixed node at  $k_c = 0$  or  $\pi$  associated with the change of network topology at hyperbola  $|w + v| = 4wv/t$  [Fig. 4(g)]. (iii) For  $\gamma = \gamma_c$  in the region  $|w + v| \geq 4wv/t$ , two loops have one fixed node except for  $w + v = \pm 1$ , the location of which does not change as the parameters  $w$  and  $v$  [Fig. 4(e)]. (iv) For  $\gamma = \gamma_c$  and  $|w + v| = 0$ , two loops have two fixed nodes [Fig. 4(f)]. The graphic eigenstates are depicted for  $\gamma > \gamma_c$  in Supplemental Material [160], where the loops detach the  $\varphi$ - $k$  torus in the broken  $\mathcal{PT}$ -symmetric phase.

The two loops are unlinked in Figs. 4(e) and 4(f); while linked in Figs. 4(g) and 4(h) due to the  $2\pi$  variation of  $\varphi_{\pm}(k)$  for each eigenstate in a  $2\pi$  period of  $k$ . This indicates the topologically nontrivial features and coincides with the winding number  $\mathcal{N}$  marked in Fig. 2(b). Both two states give identical rotating angle  $2\pi$  after  $k$  varying a period. Figures 3(a) and 3(b) depict the vector field  $\mathbf{F}_{\pm} = (\langle \sigma_x \rangle_{\pm}, \langle \sigma_y \rangle_{\pm})$ . The  $2\pi$  varying direction of the vector field yields the nontrivial topology of eigenstates and coincides with the graphic eigenstates shown in Figs. 4(g) and 4(h). The coincidence of the blue and red arrows implies the locations of EPs. The upper panel depicts the situation with single EP located at  $k_c = \pi$ ; the lower panel depicts the situation with two EPs located at  $\cos k_c = -1/4$ .

The nontrivial winding of eigenstate predicts the appearance of edge states. In topologically nontrivial gapless phase, the bands touch at zero energy and a pair of zero modes appear in the absence of gain and loss; under the  $\mathcal{CT}$  symmetry, the gapless zero modes become imaginary in the presence of gain and loss. As the gain and loss are respectively introduced in two sublattices, thus

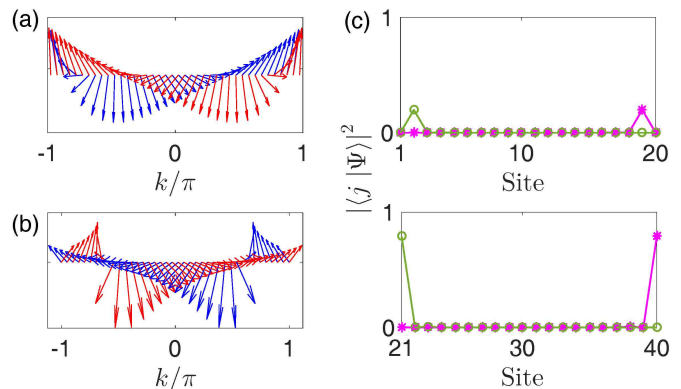


FIG. 3. Vector field  $\mathbf{F}_+(k)$  [ $\mathbf{F}_-(k)$ ] for the upper (lower) energy band represented by the blue (red) arrow at (a)  $(v, w, \gamma) = (2, 2/7, \gamma_c)$ , (b)  $(v, w, \gamma) = (3, 3/2, \gamma_c)$ ; other parameter is  $t = 1$ . (c) Gapless zero modes with amplification ( $E_{ZM} = i\gamma$ ) and attenuation ( $E_{ZM} = -i\gamma$ ) for (a),  $N = 20$ . The zero mode with amplification locates on the right. The upper and lower panels in (c) are for the upper and lower ladder legs in Fig. 2(a), respectively.

the left side and right side localized edge states confined in one sublattice experiences either an additional attenuation  $-i\gamma$  or an additional amplification  $i\gamma$ . The probability distribution of edge states is depicted in Fig. 3(c) for the situation in Fig. 3(a). The amplified edge state is appropriate for robust topological lasing.

*Conclusion.*—Real-energy topological gapless phase arising from EPs in 1D is proposed and investigated through a graphic approach. The graphic eigenstates completely encode the information of system topology and visualize the topologies of different phases in both Hermitian and non-Hermitian systems. The graph of real-energy topological gapless phase arising from EPs forms a network, its geometric topology reflects the topological properties of the ground state phase diagram. The chiral-time symmetry protects the topological gapless phase. A pair of amplification and attenuation topologically zero modes exist in the nontrivial phase. These are elucidated through a non-Hermitian SSH ladder with balanced gain and loss that directly accessible in experiment in many physical systems. Our findings propose a novel non-Hermitian topological gapless phase and provide insights into topological characterization of topological phase of matter.

This work was supported by National Natural Science Foundation of China (Grants No. 11874225 and No. 11605094).

\* jinliang@nankai.edu.cn

† songtc@nankai.edu.cn

[1] M. Z. Hasan and C. L. Kane, Colloquium: Topological

- insulators, *Rev. Mod. Phys.* **82**, 3045 (2010).
- [2] X. L. Qi and S. C. Zhang, Topological insulators and superconductors, *Rev. Mod. Phys.* **83**, 1057 (2011).
- [3] C. K. Chiu, J. C. Y. Teo, A. P. Schnyder, and S. Ryu, Classification of topological quantum matter with symmetries, *Rev. Mod. Phys.* **88**, 035005 (2016).
- [4] H. M. Weng, R. Yu, X. Hu, X. Dai, and Z. Fang, Quantum anomalous Hall effect and related topological electronic states, *Adv. Phys.* **64**, 227 (2015).
- [5] L. Lu, J. D. Joannopoulos, and M. Soljačić, Topological photonics, *Nat. Photon.* **8**, 821 (2014); Topological states in photonic systems, *Nat. Phys.* **12**, 626 (2016).
- [6] A. B. Khanikaev and G. Shvets, Two-dimensional topological photonics, *Nat. Photon.* **11**, 763 (2017).
- [7] N. Goldman, J. C. Budich, and P. Zoller, Topological quantum matter with ultracold gases in optical lattices, *Nat. Phys.* **12**, 639 (2016).
- [8] N. R. Cooper, J. Dalibard, and I. B. Spielman, Topological bands for ultracold atoms, *Rev. Mod. Phys.* **91**, 015005 (2019).
- [9] T. Ozawa, H. M. Price, A. Amo, N. Goldman, M. Hafezi, L. Lu, M. Rechtsman, D. Schuster, J. Simon, O. Zilberberg, and I. Carusotto, Topological photonics, *Rev. Mod. Phys.* **91**, 015006 (2019).
- [10] M. Hafezi, E. A. Demler, M. D. Lukin, and J. M. Taylor, Robust optical delay lines with topological protection, *Nat. Phys.* **7**, 907 (2011); M. Hafezi, S. Mittal, J. Fan, A. Migdall, and J. M. Taylor, Imaging topological edge states in silicon photonics, *Nat. Photon.* **7**, 1001 (2013).
- [11] M. C. Rechtsman, J. M. Zeuner, Y. Plotnik, Y. Lumer, D. Podolsky, F. Dreisow, S. Nolte, M. Segev, and A. Szameit, Photonic Floquet topological insulators, *Nature (London)* **496**, 196 (2013).
- [12] W.-J. Chen, S.-J. Jiang, X.-D. Chen, B. Zhu, L. Zhou, J.-W. Dong, and C. T. Chan, Experimental realization of photonic topological insulator in a uniaxial metacrytal waveguide, *Nat. Commun.* **5**, 5782 (2014).
- [13] S. Mukherjee, A. Spracklen, M. Valiente, E. Andersson, P. Öhberg, N. Goldman, and R. R. Thomson, Experimental observation of anomalous topological edge modes in a slowly driven photonic lattice, *Nat. Commun.* **8**, 13918 (2017).
- [14] M. A. Bandres, M. C. Rechtsman, and M. Segev, Topological Photonic Quasicrystals: Fractal Topological Spectrum and Protected Transport, *Phys. Rev. X* **6**, 011016 (2016).
- [15] Q. Lin, M. Xiao, L. Yuan, and S. Fan, Photonic Weyl point in a twodimensional resonator lattice with a synthetic frequency dimension, *Nat. Commun.* **7**, 13731 (2016).
- [16] D. Leykam and Y. D. Chong, Edge Solitons in Nonlinear Photonic Topological Insulators, *Phys. Rev. Lett.* **117**, 143901 (2016).
- [17] J.-W. Dong, X.-D. Chen, H. Zhu, Y. Wang, and X. Zhang, Valley photonic crystals for control of spin and topology, *Nat. Mater.* **16**, 298 (2017).
- [18] J. Noh, S. Huang, D. Leykam, Y. D. Chong, K. P. Chen, M. C. Rechtsman, Experimental observation of optical Weyl points and Fermi arc-like surface states, *Nat. Phys.* **13**, 611 (2017).
- [19] S. Mittal, J. Fan, S. Faez, A. Migdall, J. M. Taylor, and M. Hafezi, Topologically Robust Transport of Photons in a Synthetic Gauge Field, *Phys. Rev. Lett.* **113**, 087403 (2014); S. Mittal, S. Ganeshan, J. Fan, A. Vaezi, and M. Hafezi, Measurement of topological invariants in a 2D photonic system, *Nat. Photon.* **10**, 180 (2016); S. Mittal, E. A. Goldschmidt, and M. Hafezi, A topological source of quantum light, *Nature* **561**, 502 (2018).
- [20] S. Klemmt, T. H. Harder, O. A. Egorov, K. Winkler, R. Ge, M. A. Bandres, M. Emmerling, L. Worschech, T. C. H. Liew, M. Segev, C. Schneider, and S. Höfling, Exciton-polariton topological insulator, *Nature* **562**, 552 (2018).
- [21] L. Fu and C. L. Kane, Superconducting Proximity Effect and Majorana Fermions at the Surface of a Topological Insulator, *Phys. Rev. Lett.* **100**, 096407 (2008).
- [22] R. M. Lutchyn, J. D. Sau, and S. D. Sarma, Majorana Fermions and a Topological Phase Transition in Semiconductor-Superconductor Heterostructures, *Phys. Rev. Lett.* **105**, 077001 (2010).
- [23] V. Mourik, K. Zuo, S. M. Frolov, S. R. Plissard, E. P. A. M. Bakkers, and L. P. Kouwenhoven, Signatures of Majorana Fermions in Hybrid Superconductor-Semiconductor Nanowire Devices, *Science* **336**, 1003 (2012); S. N. Perge, I. K. Drozdov, J. Li, H. Chen, S. Jeon, J. Seo, A. H. MacDonald, B. A. Bernevig, and A. Yazdani, Observation of Majorana fermions in ferromagnetic atomic chains on a superconductor, *Science* **346**, 602 (2014).
- [24] Y. Oreg, G. Refael, and F. von Oppen, Helical Liquids and Majorana Bound States in Quantum Wires, *Phys. Rev. Lett.* **105**, 177002 (2010).
- [25] A. H. C. Neto, F. Guinea, N. M. R. Peres, K. S. Novoselov, and A. K. Geim, The electronic properties of graphene, *Rev. Mod. Phys.* **81**, 109 (2009).
- [26] J. A. Steinberg, S. M. Young, S. Zaheer, C. L. Kane, E. J. Mele, and A. M. Rappe, Bulk Dirac Points in Distorted Spinels, *Phys. Rev. Lett.* **112**, 036403 (2014).
- [27] J. Xiong, S. K. Kushwaha, T. Liang, J. W. Krizan, M. Hirschberger, W. Wang, R. J. Cava, and N. P. Ong, Evidence for the chiral anomaly in the Dirac semimetal  $\text{Na}_3\text{Bi}$ , *Science* **350**, 413 (2015).
- [28] Z. K. Liu, J. Jiang, B. Zhou, Z. J. Wang, Y. Zhang, H. M. Weng, D. Prabhakaran, S.-K. Mo, H. Peng, P. Dudin, T. Kim, M. Hoesch, Z. Fang, X. Dai, Z. X. Shen, D. L. Feng, Z. Hussain, and Y. L. Chen, A stable three-dimensional topological Dirac semimetal  $\text{Cd}_3\text{As}_2$ , *Nat. Mater.* **13**, 677 (2014); Z. K. Liu, B. Zhou, Y. Zhang, Z. J. Wang, H. M. Weng, D. Prabhakaran, S. K. Mo, Z. X. Shen, Z. Fang, X. Dai, Z. Hussain, and Y. L. Chen, Discovery of a Three-Dimensional Topological Dirac Semimetal,  $\text{Na}_3\text{Bi}$ , *Science* **343**, 864 (2014).
- [29] S. M. Young, S. Zaheer, J. C. Y. Teo, C. L. Kane, E. J. Mele, and A. M. Rappe, Dirac Semimetal in Three Dimensions, *Phys. Rev. Lett.* **108**, 140405 (2012).
- [30] Z. J. Wang, Y. Sun, X. Q. Chen, C. Franchini, G. Xu, H. M. Weng, X. Dai, and Z. Fang, Dirac semimetal and topological phase transitions in  $\text{A}_3\text{Bi}$  ( $\text{A}=\text{Na}, \text{K}, \text{Rb}$ ), *Phys. Rev. B* **85**, 195320 (2012).
- [31] B. Q. Lv, N. Xu, H. M. Weng, J. Z. Ma, P. Richard, X. C. Huang, L. X. Zhao, G. F. Chen, C. E. Matt, F. Bisti, V. N. Strocov, J. Mesot, Z. Fang, X. Dai, T. Qian, M. Shi, and H. Ding, Observation of Weyl nodes in  $\text{TaAs}$ , *Nat. Phys.* **11**, 724 (2015).
- [32] M. Hirschberger, S. Kushwaha, Z. J. Wang, Q. Gibson, S. H. Liang, C. A. Belvin, B. A. Bernevig, R. J. Cava, and N. P. Ong, The chiral anomaly and thermopower of

- Weyl fermions in the half-Heusler GdPtBi, *Nat. Mater.* **15**, 1161 (2016); H. M. Weng, C. Fang, Z. Fang, B. A. Bernevig, and X. Dai, Weyl Semimetal Phase in Noncentrosymmetric Transition-Metal Monophosphides, *Phys. Rev. X* **5**, 011029 (2015).
- [33] S. M. Huang, S. Y. Xu, I. Belopolski, C. C. Lee, G. Q. Chang, B. K. Wang, N. Alidoust, G. Bian, M. Neupane, C. Zhang, S. Jia, A. Bansil, H. Lin, and M. Z. Hasan, A Weyl Fermion semimetal with surface Fermi arcs in the transition metal monpnictide TaAs class, *Nat. Commun.* **6**, 7373 (2015).
- [34] S. Y. Xu, I. Belopolski, N. Alidoust, M. Neupane, G. Bian, C. L. Zhang, R. Sankar, G. Q. Chang, Z. J. Yuan, C. C. Lee, S. M. Huang, H. Zheng, J. Ma, D. S. Sanchez, B. K. Wang, A. Bansil, F. C. Chou, P. P. Shibayev, H. Lin, S. Jia, and M. Z. Hasan, Discovery of a Weyl fermion semimetal and topological Fermi arcs, *Science* **349**, 613 (2015).
- [35] N. P. Armitage, E. J. Mele, and A. Vishwanath, Weyl and Dirac semimetals in three-dimensional solids, *Rev. Mod. Phys.* **90**, 015001 (2018).
- [36] K. Y. Yang, Y. M. Lu, and Y. Ran, Quantum Hall effects in a Weyl semimetal: Possible application in pyrochlore iridates, *Phys. Rev. B* **84**, 075129 (2011).
- [37] A. A. Burkov and L. Balents, Weyl Semimetal in a Topological Insulator Multilayer, *Phys. Rev. Lett.* **107**, 127205 (2011).
- [38] G. Xu, H. Weng, Z. Wang, X. Dai, and Z. Fang, Chern Semimetal and the Quantized Anomalous Hall Effect in  $\text{HgCr}_2\text{Se}_4$ , *Phys. Rev. Lett.* **107**, 186806 (2011).
- [39] W. W. Krempa and Y. B. Kim, Topological and magnetic phases of interacting electrons in the pyrochlore iridates, *Phys. Rev. B* **85**, 045124 (2012).
- [40] Z. Wang, H. Weng, Q. Wu, X. Dai, and Z. Fang, Three-dimensional Dirac semimetal and quantum transport in  $\text{Cd}_3\text{As}_2$ , *Phys. Rev. B* **88**, 125427 (2013).
- [41] J. M. Hou, Hidden-Symmetry-Protected Topological Semimetals on a Square Lattice, *Phys. Rev. Lett.* **111**, 130403 (2013).
- [42] K. Sun, W. V. Liu, A. Hemmerich, and S. D. Sarma, Topological semimetal in a fermionic optical lattice, *Nat. Phys.* **8**, 67 (2012).
- [43] M. Neupane, S. Y. Xu, R. Sankar, N. Alidoust, G. Bian, C. Liu, I. Belopolski, T. R. Chang, H. T. Jeng, H. Lin, A. Bansil, F. C. Chou, and M. Z. Hasan, Observation of a three-dimensional topological Dirac semimetal phase in high-mobility  $\text{Cd}_3\text{As}_2$ , *Nat. Commun.* **5**, 3786 (2014).
- [44] L. Lu, Z. Y. Wang, D. X. Ye, L. X. Ran, L. Fu, J. D. Joannopoulos, and M. Soljačić, Experimental observation of Weyl points, *Science* **349**, 622 (2015).
- [45] C. Li, S. Lin, G. Zhang, and Z. Song, Topological nodal points in two coupled Su-Schrieffer-Heeger chains, *Phys. Rev. B* **96**, 125418 (2017).
- [46] C. M. Bender and S. Boettcher, Real Spectra in non-Hermitian Hamiltonians Having  $\mathcal{PT}$  Symmetry, *Phys. Rev. Lett.* **80**, 5243 (1998).
- [47] A. Mostafazadeh, Pseudo-Hermiticity versus  $\mathcal{PT}$ -symmetry: The necessary condition for the reality of the spectrum of a non-Hermitian Hamiltonian, *J. Math. Phys.* **43**, 205 (2002).
- [48] N. Moiseyev, *Non-Hermitian Quantum Mechanics* (Cambridge University Press, Cambridge, UK, 2011).
- [49] A. Ruschhaupt, F. Delgado, and J. G. Muga, Physical realization of  $\mathcal{PT}$ -symmetric potential scattering in a planar slab waveguide, *J. Phys. A* **38**, L171 (2005).
- [50] S. Klaiman, U. Guenther, and N. Moiseyev, Visualization of Branch Points in  $\mathcal{PT}$ -Symmetric Waveguides, *Phys. Rev. Lett.* **101**, 080402 (2008).
- [51] R. El-Ganainy, K. G. Makris, D. N. Christodoulides, and Z. H. Musslimani, *Opt. Lett.* **32**, 2632 (2007); K. G. Makris, R. El-Ganainy, D. N. Christodoulides, and Z. H. Musslimani, Beam Dynamics in  $\mathcal{PT}$  Symmetric Optical Lattices, *Phys. Rev. Lett.* **100**, 103904 (2008); Z. H. Musslimani, K. G. Makris, R. El-Ganainy, and D. N. Christodoulides, Optical Solitons in  $\mathcal{PT}$  Periodic Potentials, *Phys. Rev. Lett.* **100**, 030402 (2008).
- [52] A. Guo, G. J. Salamo, D. Duchesne, R. Morandotti, M. Volatier-Ravat, V. Aimez, G. A. Siviloglou, and D. N. Christodoulides, Observation of  $\mathcal{PT}$ -Symmetry Breaking in Complex Optical Potentials, *Phys. Rev. Lett.* **103**, 093902 (2009).
- [53] C. E. Rüter, K. G. Makris, R. El-Ganainy, D. N. Christodoulides, M. Segev, and D. Kip, Observation of parity-time symmetry in optics, *Nat. Phys.* **6**, 192 (2010).
- [54] B. Peng, S. K. Özdemir, F. Lei, F. Monifi, M. Gianfreda, G. L. Long, S. Fan, F. Nori, C. M. Bender and L. Yang, Parity-time-symmetric whispering-gallery microcavities, *Nat. Phys.* **10**, 394 (2014).
- [55] L. Chang, X. Jiang, S. Hua, C. Yang, J. Wen, L. Jiang, G. Li, G. Wang and M. Xiao, Parity-time symmetry and variable optical isolation in active-passive-coupled microresonators, *Nat. Photon.* **8**, 524 (2014).
- [56] L. Feng, Z. J. Wong, R. M. Ma, Y. Wang, and X. Zhang, Single-mode laser by parity-time symmetry breaking, *Science* **346**, 972 (2014).
- [57] R. Fleury, D. Sounas, and A. Alù, An invisible acoustic sensor based on parity-time symmetry, *Nat. Commun.* **6**, 5905 (2015).
- [58] K. G. Makris, Z. H. Musslimani, D. N. Christodoulides, and S. Rotter, Constant-intensity waves and their modulation instability in non-Hermitian potentials, *Nat. Commun.* **6**, 7257 (2015).
- [59] L. Feng, R. El-Ganainy, and L. Ge, Non-Hermitian photonics based on parity-time symmetry, *Nat. Photo.* **11**, 752 (2017).
- [60] R. El-Ganainy, K. G. Makris, M. Khajavikhan, Z. H. Musslimani, S. Rotter and D. N. Christodoulides, Non-Hermitian physics and  $\mathcal{PT}$  symmetry, *Nat. Phys.* **14**, 11 (2018).
- [61] S. K. Gupta, Y. Zou, X. Y. Zhu, M. H. Lu, L. J. Zhang, X. P. Liu, and Y. F. Chen, Parity-time Symmetry in Non-Hermitian Complex Media, arXiv:1803.00794.
- [62] C. Dembowski, H. D. Graf, H. L. Harney, A. Heine, W. D. Heiss, H. Rehfeld, and A. Richter, Experimental Observation of the Topological Structure of Exceptional Points, *Phys. Rev. Lett.* **86**, 787 (2001); C. Dembowski, B. Dietz, H. D. Graf, H. L. Harney, A. Heine, W. D. Heiss, and A. Richter, Encircling an exceptional point, *Phys. Rev. E* **69**, 056216 (2004).
- [63] W. D. Heiss and H. L. Harney, The chirality of exceptional points, *Eur. Phys. J. D* **17**, 149 (2001); W. D. Heiss, Exceptional points of non-Hermitian operators, *J. Phys. A* **37**, 2455 (2004); M. V. Berry, Physics of non-hermitian degeneracies, *Czech. J. Phys.* **54**, 1039 (2004).
- [64] R. Uzdin, A. Mailybaev, and N. Moiseyev, On the observability and asymmetry of adiabatic state flips gen-

- erated by exceptional points, *J. Phys. A* **44**, 435302 (2011).
- [65] B. Zhen, C. W. Hsu, Y. Igarashi, L. Lu, I. Kaminer, A. Pick, S. L. Chua, J. D. Joannopoulos and M. Soljačić, Spawning rings of exceptional points out of Dirac cones, *Nature* **525**, 354 (2015).
- [66] J. Doppler, A. A. Mailybaev, J. Bohm, U. Kuhl, A. Girschik, F. Libisch, T. J. Milburn, P. Rabl, N. Moiseyev and S. Rotter, Dynamically encircling an exceptional point for asymmetric mode switching, *Nature* **537**, 76 (2016).
- [67] H. Xu, D. Mason, L. Jiang, and J. G. E. Harris, Topological energy transfer in an optomechanical system with exceptional points, *Nature* **537**, 80 (2016).
- [68] J. Wiersig, Enhancing the Sensitivity of Frequency and Energy Splitting Detection by Using Exceptional Points: Application to Microcavity Sensors for Single Particle Detection, *Phys. Rev. Lett.* **112**, 203901 (2014).
- [69] Z. P. Liu, J. Zhang, S. K. Özdemir, B. Peng, H. Jing, X. Y. Lü, C. W. Li, L. Yang, F. Nori, and Y. X. Liu, *Phys. Rev. Lett.* **117**, 110802 (2016).
- [70] W. Chen, S. K. Özdemir, G. Zhao, J. Wiersig, and L. Yang, Exceptional points enhance sensing in an optical microcavity, *Nature* **548**, 192 (2017).
- [71] H. Hodaei, A. U. Hassan, S. Wittek, H. Garcia-Gracia, R. El-Ganainy, D. N. Christodoulides and M. Khajavikhan, Enhanced sensitivity at higher-order exceptional points, *Nature* **548**, 187 (2017).
- [72] K. Ding, G. Ma, M. Xiao, Z. Q. Zhang, and C. T. Chan, Emergence, Coalescence, and Topological Properties of Multiple Exceptional Points and Their Experimental Realization, *Phys. Rev. X* **6**, 021007 (2016).
- [73] K. Ding, G. Ma, Z. Q. Zhang, and C. T. Chan, Experimental Demonstration of an Anisotropic Exceptional Point, *Phys. Rev. Lett.* **121**, 085702 (2018).
- [74] X. L. Zhang, S. B. Wang, B. Hou, and C. T. Chan, Dynamically Encircling Exceptional Points: In situ Control of Encircling Loops and the Role of the Starting Point, *Phys. Rev. X* **8**, 021066 (2018).
- [75] Q. Zhong, D. N. Christodoulides, M. Khajavikhan, K. G. Makris, and R. El-Ganainy, Power-law scaling of extreme dynamics near higher-order exceptional points, *Phys. Rev. A* **97**, 020105(R) (2018).
- [76] B. Midya, H. Zhao, and Feng, L. Non-Hermitian photonics promises exceptional topology of light, *Nat. Commun.* **9**, 2674 (2018).
- [77] M. A. Miri and A. Alù, Exceptional points in optics and photonics, *Science* **363**, eaar7709 (2019).
- [78] M. S. Rudner and L. S. Levitov, Topological transition in a non-hermitian quantum walk, *Phys. Rev. Lett.* **102**, 065703 (2009); M. S. Rudner, M. Levin, and L. S. Levitov, Survival, decay, and topological protection in non-Hermitian quantum transport, arXiv:1605.07652.
- [79] S. Diehl, E. Rico, M. A. Baranov, and P. Zoller, Topology by dissipation in atomic quantum wires, *Nat. Phys.* **7**, 971 (2011).
- [80] Y. C. Hu and T. L. Hughes, Absence of topological insulator phases in non-Hermitian  $\mathcal{PT}$ -symmetric Hamiltonians, *Phys. Rev. B* **84**, 153101 (2011); K. Esaki, M. Sato, K. Hasebe, and M. Kohmoto, Edge states and topological phases in non-Hermitian systems, *Phys. Rev. B* **84**, 205128 (2011).
- [81] H. Schomerus, Topologically protected midgap states in complex photonic lattices, *Opt. Lett.* **38**, 1912 (2013).
- [82] J. M. Zeuner, M. C. Rechtsman, Y. Plotnik, Y. Lumer, S. Nolte, M. S. Rudner, M. Segev, and A. Szameit, Observation of a topological transition in the bulk of a non-Hermitian system, *Phys. Rev. Lett.* **115**, 040402 (2015).
- [83] C. He, X. C. Sun, X. P. Liu, M. H. Lu, Y. Chen, L. Feng, and Y. F. Chen, Photonic topological insulator with broken time-reversal symmetry, *Proc. Natl. Acad. Sci. U.S.A.* **113**, 4924 (2016).
- [84] W. Zhu, X. Fang, D. Li, Y. Sun, Y. Li, Y. Jing, and H. Chen, Simultaneous observation of a topological edge state and exceptional point in an open and non-Hermitian acoustic system, *Phys. Rev. Lett.* **121**, 124501 (2018).
- [85] H. Zhao, S. Longhi, and L. Feng, Robust light state by quantum phase transition in non-Hermitian optical materials, *Sci. Rep.* **5**, 17022 (2015); B. Midya and L. Feng, Topological multiband photonic superlattices, *Phys. Rev. A* **98**, 043838 (2018).
- [86] G. Q. Liang and Y. D. Chong, Optical resonator analog of a two-dimensional topological insulator, *Phys. Rev. Lett.* **110**, 203904 (2013).
- [87] W. Hu, H. Wang, P. P. Shum, and Y. D. Chong, Exceptional points in a non-Hermitian topological pump, *Phys. Rev. B* **95**, 184306 (2017); Y. Chen and H. Zhai, Hall Conductance of a Non-Hermitian Chern Insulator, *Phys. Rev. B* **98**, 245130 (2018); T. Rakovszky, J. K. Asbóth, and A. Alberti, Detecting topological invariants in chiral symmetric insulators via losses, *Phys. Rev. B* **95**, 201407(R) (2017); T. M. Philip, M. R. Hirsbrunner, and M. J. Gilbert, Loss of Hall conductivity quantization in a non-Hermitian quantum anomalous Hall insulator, *Phys. Rev. B* **98**, 155430 (2018).
- [88] C. Yin, H. Jiang, L. Li, R. Lü, and S. Chen, Geometrical meaning of winding number and its characterization of topological phases in one-dimensional chiral non-Hermitian systems, *Phys. Rev. A* **97**, 052115 (2018); H. Jiang, C. Yang, and S. Chen, Topological invariants and phase diagrams for one-dimensional two-band non-Hermitian systems without chiral symmetry, *Phys. Rev. A* **98**, 052116 (2018); H. Jiang, L. J. Lang, C. Yang, S. L. Zhu, and S. Chen, Interplay of non-Hermitian skin effects and Anderson localization in non-reciprocal quasiperiodic lattices, arXiv:1901.09399.
- [89] J. Gong and Q. H. Wang, Stabilizing non-Hermitian systems by periodic driving, *Phys. Rev. A* **91**, 042135 (2015); L. Zhou, Q. H. Wang, H. Wang, and J. Gong, Dynamical quantum phase transitions in non-Hermitian lattices, *Phys. Rev. A* **98**, 022129 (2018).
- [90] R. Wang, X. Z. Zhang, and Z. Song, Dynamical topological invariant for non-Hermitian Rice-Mele model, *Phys. Rev. A* **98**, 042120 (2018); X. Z. Zhang and Z. Song, Partial topological Zak phase and dynamical confinement in a non-Hermitian bipartite system, *Phys. Rev. A* **99**, 012113 (2019).
- [91] H. Shen and L. Fu, Quantum Oscillation from in-gap states and a non-Hermitian Landau level problem, *Phys. Rev. Lett.* **121**, 026403 (2018).
- [92] K. Takata and M. Notomi, Photonic topological insulating phase induced solely by gain and loss, *Phys. Rev. Lett.* **121**, 213902 (2018).
- [93] Q. B. Zeng, Y. B. Yang, and Y. Xu, Topological Non-Hermitian Quasicrystals, arXiv:1901.08060.

- [94] T. Yoshida, R. Peters, and N. Kawakami, Non-Hermitian perspective of the band structure in heavy fermion systems, *Phys. Rev. B* **98**, 035141 (2018); K. Yokomizo and S. Murakami, Bloch Band Theory for Non-Hermitian Systems, arXiv:1902.10958; Z. Y. Ge, Y. R. Zhang, T. Liu, S. W. Li, H. Fan, and F. Nori, Topological band theory for non-Hermitian systems from a quantum field viewpoint, arXiv:1903.09985.
- [95] C. Yuce, Topological phase in a non-Hermitian  $\mathcal{PT}$  symmetric system, *Phys. Lett. A* **379**, 1213 (2015); Majorana edge modes with gain and loss, *Phys. Rev. A* **93**, 062130 (2016); Edge states at the interface of non-Hermitian systems, *Phys. Rev. A* **97**, 042118 (2018); Stable topological edge states in a non-Hermitian four-band model, *Phys. Rev. A* **98**, 012111 (2018).
- [96] S. Lieu, Topological phases in the non-Hermitian Su-Schrieffer-Heeger model, *Phys. Rev. B* **97**, 045106 (2018); Topological symmetry classes for non-Hermitian models and connections to the bosonic Bogoliubov-de Gennes equation, *Phys. Rev. B* **98**, 115135 (2018).
- [97] H. Menke and M. M. Hirschmann, Topological quantum wires with balanced gain and loss, *Phys. Rev. B* **95**, 174506 (2017).
- [98] J. Carlström and E. J. Bergholtz, Exceptional links and twisted Fermi ribbons in non-Hermitian systems, *Phys. Rev. A* **98**, 042114 (2018); J. Carlström, M. Stalhammar, J. C. Budich, and E. J. Bergholtz, Knotted Non-Hermitian Metals, *Phys. Rev. B* **99**, 161115(R) (2019).
- [99] K. Kawabata, K. Shiozaki, and M. Ueda, Anomalous helical edge states in a non-Hermitian Chern insulator, *Phys. Rev. B* **98**, 165148 (2018).
- [100] J. Hou, Z. Li, X. W. Luo, Q. Gu, and C. Zhang, Topological bands and triply-degenerate points in non-Hermitian hyperbolic metamaterials, arXiv:1808.06972.
- [101] B. X. Wang and C. Y. Zhao, Topological phonon polaritons in one-dimensional non-Hermitian silicon carbide nanoparticle chains, *Phys. Rev. B* **98**, 165435 (2018); Topological photonic states in one-dimensional dimerized ultracold atomic chains, *Phys. Rev. A* **98**, 023808 (2018).
- [102] A. A. Zyuzin and A. Yu. Zyuzin, Flat band in disorder-driven non-Hermitian Weyl semimetals, *Phys. Rev. B* **97**, 041203(R) (2018); K. Moors, A. A. Zyuzin, A. Y. Zyuzin, R. P. Tiwari, and T. L. Schmidt, Disorder-driven exceptional lines and Fermi ribbons in tilted nodal-line semimetals, *Phys. Rev. B* **99**, 041116(R) (2019); V. M. Martinez Alvarez and M. D. Coutinho-Filho, Edge states in trimer lattices, *Phys. Rev. A* **99**, 013833 (2019).
- [103] F. K. Kunst and V. Dwivedi, Non-Hermitian systems and topology: A transfer matrix perspective, arXiv:1812.02186; F. K. Kunst, G. van Miert, and E. J. Bergholtz, Extended Bloch theorem for topological lattice models with open boundaries, arXiv:1812.03099.
- [104] L. Herviou, J. H. Bardarson, and N. Regnault, Impact of Ground Truth Annotation Quality on Performance of Semantic Image Segmentation of Traffic Conditions, arXiv:1901.00001; H. G. Zirnstein, G. Refael, and B. Rosenow, Bulk-boundary correspondence for non-Hermitian Hamiltonians via Green functions, arXiv:1901.11241; M. R. Hirsbrunner, T. M. Philip, and M. J. Gilbert, Topology and Observables of the Non-Hermitian Chern Insulator, arXiv:1901.09961.
- [105] W. B. Rui, Y. X. Zhao, and A. P. Schnyder, Classification of massive Dirac models with generic non-Hermitian perturbations, arXiv: 1902.06617.
- [106] A. Ghatak and T. Das, New topological invariants in non-Hermitian systems, *J. Phys.: Condens. Matter* **31**, 263001 (2019).
- [107] T. Ohashi, S. Kobayashi, and Y. Kawaguchi, Generalized Berry phase for a bosonic Bogoliubov system with exceptional points, arXiv:1904.08724.
- [108] S. Malzard, C. Poli, and H. Schomerus, Topologically Protected Defect States in Open Photonic Systems with Non-Hermitian Charge-Conjugation and Parity-Time Symmetry, *Phys. Rev. Lett.* **115**, 200402 (2015).
- [109] L. Jin, Topological phases and edge states in a non-Hermitian trimerized optical lattice, *Phys. Rev. A* **96**, 032103 (2017); L. Jin, P. Wang, and Z. Song, Su-Schrieffer-Heeger chain with one pair of  $\mathcal{PT}$ -symmetric defects, *Sci. Rep.* **7**, 5903 (2017).
- [110] S. Lin and Z. Song, Wide-range-tunable Dirac-cone band structure in a chiral-time-symmetric non-Hermitian system, *Phys. Rev. A* **96**, 052121 (2017).
- [111] L. Xiao, X. Zhan, Z. H. Bian, K. K. Wang, X. Zhang, X. P. Wang, J. Li, K. Mochizuki, D. Kim, N. Kawakami, W. Yi, H. Obuse, B. C. Sanders, and P. Xue, Observation of topological edge states in parity-time-symmetric quantum walks, *Nat. Phys.* **13**, 1117 (2017).
- [112] K. Kawabata, Y. Ashida, H. Katsura, and M. Ueda, Parity-time-symmetric topological superconductor, *Phys. Rev. B* **98**, 085116 (2018); X. Ni, D. Smirnova, A. Poddubny, D. Leykam, Y. Chong, and A. B. Khanikaev,  $\mathcal{PT}$  phase transitions of edge states at  $\mathcal{PT}$  symmetric interfaces in non-Hermitian topological insulators, *Phys. Rev. B* **98**, 165129 (2018); A. Ghatak and T. Das, Theory of superconductivity with non-Hermitian and parity-time reversal symmetric Cooper pairing symmetry, *Phys. Rev. B* **97**, 014512 (2018).
- [113] L. J. Lang, Y. Wang, H. Wang, and Y. D. Chong, Effects of non-Hermiticity on Su-Schrieffer-Heeger defect states, *Phys. Rev. B* **98**, 094307 (2018).
- [114] T. T. Koutserimpas, A. Alù, and R. Fleury, Parametric amplification and bidirectional invisibility in  $\mathcal{PT}$  symmetric time-Floquet systems, *Phys. Rev. A* **97**, 013839 (2018).
- [115] E. Cancellieri and H. Schomerus, PC-symmetry protected edge states in interacting driven-dissipative bosonic systems, *Phys. Rev. A* **99**, 033801 (2019); J. Hou, Z. Li, Q. Gu, and C. Zhang, Non-Hermitian Photonics based on Charge-Parity Symmetry, arXiv:1904.05260.
- [116] A. Yoshida, Y. Ohtaki, R. Ohtaki, and T. Fukui, Edge states, corner states, and flat bands in a two-dimensional  $\mathcal{PT}$  symmetric system, arXiv:1904.05007.
- [117] Y. Xu, S. T. Wang, and L. M. Duan, Weyl exceptional rings in a three-dimensional dissipative cold atomic gas, *Phys. Rev. Lett.* **118**, 045701 (2017).
- [118] D. Leykam, K. Y. Bliokh, C. Huang, Y. D. Chong, and F. Nori, Edge modes, degeneracies, and topological numbers in non-Hermitian systems, *Phys. Rev. Lett.* **118**, 040401 (2017).
- [119] H. Shen, B. Zhen, and L. Fu, Topological band theory for non-Hermitian Hamiltonians, *Phys. Rev. Lett.* **120**, 146402 (2018).
- [120] C. Poli, M. Bellec, U. Kuhl, F. Mortessagne, and H. Schomerus, Selective enhancement of topologically induced interface states in a dielectric resonator chain,



- Nat. Commun. **6**, 6710 (2015).
- [121] S. Weimann, M. Kremer, Y. Plotnik, Y. Lumer, S. Nolte, K. G. Makris, M. Segev, M. C. Rechtsman, and A. Szameit, Topologically protected bound states in photonic parity–time-symmetric crystals, Nat. Mater. **16**, 433 (2017).
- [122] M. Pan, H. Zhao, P. Miao, S. Longhi, and L. Feng, Photonic zero mode in a non-Hermitian photonic lattice, Nat. Commun. **9**, 1308 (2018).
- [123] P. St-Jean, V. Goblot, E. Galopin, A. Lemaitre, T. Ozawa, L. Le Gratiet, I. Sagnes, J. Bloch, and A. Amo, Lasing in topological edge states of a one-dimensional lattice, Nat. Photon **11**, 651 (2017).
- [124] M. Parto, S. Wittek, H. Hodaei, G. Harari, M. A. Bandres, J. Ren, M. C. Rechtsman, M. Segev, D. N. Christodoulides, and M. Khajavikhan, Edge-mode lasing in 1D topological active arrays, Phys. Rev. Lett. **120**, 113901 (2018).
- [125] H. Zhao, P. Miao, M. H. Teimourpour, S. Malzard, R. El-Ganainy, H. Schomerus, and L. Feng, Topological hybrid silicon microlasers, Nat. Commun. **9**, 981 (2018).
- [126] G. Harari, M. A. Bandres, Y. Lumer, M. C. Rechtsman, Y. D. Chong, M. Khajavikhan, D. N. Christodoulides, and M. Segev, Topological insulator laser: Theory, Science **359**, eaar4003 (2018); M. A. Bandres, S. Wittek, G. Harari, M. Parto, J. Ren, M. Segev, D. Christodoulides, and M. Khajavikhan, Topological insulator laser: Experiments, Science **359**, eaar4005 (2018).
- [127] Y. V. Kartashov and D. V. Skryabin, Two-Dimensional Topological Polariton Laser, Phys. Rev. Lett. **122**, 083902 (2019).
- [128] M. Seclì, M. Capone, and I. Carusotto, Theory of chiral edge state lasing in a two-dimensional topological system, arXiv:1901.01290.
- [129] T. Liu, Y. R. Zhang, Q. Ai, Z. Gong, K. Kawabata, M. Ueda, and F. Nori, Second-order topological phases in non-Hermitian systems, Phys. Rev. Lett. **122**, 076801 (2018).
- [130] M. Ezawa, Non-Hermitian boundary and interface states in nonreciprocal higher-order topological metals and electrical circuits, Phys. Rev. B **99**, 121411(R) (2019); Electric-circuit realization of non-Hermitian higher-order topological systems, arXiv:1810.04527.
- [131] C. H. Lee, L. Li, and J. Gong, Hybrid higher-order skin-topological modes in non-reciprocal systems, arXiv:1810.11824.
- [132] X. W. Luo and C. Zhang, Higher-order topological corner states induced by gain and loss, arXiv:1903.02448.
- [133] E. Edvardsson, F. K. Kunst, and E. J. Bergholtz, Non-Hermitian extensions of higher-order topological phases and their biorthogonal bulk-boundary correspondence, Phys. Rev. B **99**, 081302(R) (2019).
- [134] T. E. Lee, Anomalous edge state in a non-Hermitian lattice, Phys. Rev. Lett. **116**, 133903 (2016); Y. Xiong, Why does bulk boundary correspondence fail in some non-hermitian topological models, J. Phys. Commun. **2**, 035043 (2018).
- [135] V. M. Martinez Alvarez, J. E. Barrios Vargas, and L. E. F. Foa Torres, Non-Hermitian robust edge states in one dimension: Anomalous localization and eigenspace condensation at exceptional points, Phys. Rev. B **97**, 121401(R) (2018); V. M. Martinez Alvarez, J. E. Barrios Vargas, M. Berdakin, and L. E. F. Foa Torres, Topological states of non-Hermitian systems, Eur. Phys. J. Spec. Top. **227**, 1295 (2018).
- [136] S. Yao and Z. Wang, Edge states and topological invariants of non-Hermitian systems, Phys. Rev. Lett. **121**, 086803 (2018); S. Yao, F. Song, and Z. Wang, Non-hermitian Chern bands, Phys. Rev. Lett. **121**, 136802 (2018); F. K. Kunst, E. Edvardsson, J. C. Budich, and E. J. Bergholtz, Biorthogonal bulk-boundary correspondence in non-Hermitian systems, Phys. Rev. Lett. **121**, 026808 (2018).
- [137] L. Jin and Z. Song, Bulk-boundary correspondence in a non-Hermitian system in one dimension with chiral inversion symmetry, Phys. Rev. B **99**, 081103(R) (2019).
- [138] Z. Yang and J. Hu, Non-Hermitian Hopf-link exceptional line semimetals, Phys. Rev. B **99**, 081102(R) (2019).
- [139] H. Wang, J. Ruan, and H. Zhang, Non-Hermitian nodal-line semimetals with an anomalous bulk-boundary correspondence, Phys. Rev. B **99**, 075130 (2019).
- [140] C. H. Lee and R. Thomale, Anatomy of skin modes and topology in non-Hermitian systems, arXiv:1809.02125; C. H. Lee, G. Li, Y. Liu, T. Tai, R. Thomale, and X. Zhang, Tidal surface states as fingerprints of non-Hermitian nodal knot metals, arXiv:1812.02011.
- [141] K. Luo, J. Feng, Y. X. Zhao, and R. Yu, Nodal Manifolds Bounded by Exceptional Points on Non-Hermitian Honeycomb Lattices and Electrical-Circuit Realizations, arXiv:1810.09231; D. S. Borgnia, A. J. Kruchkov, and R. J. Slager, Non-Hermitian Boundary Modes, arXiv:1902.07217; T.-S. Deng and W. Yi, Non-Bloch topological invariants in a non-Hermitian domain-wall system, arXiv: 1903.03811; F. Song, S. Yao, and Z. Wang, Non-Hermitian skin effect and chiral damping in open quantum systems, arXiv: 1904.08432.
- [142] Z. P. Gong, Y. Ashida, K. Kawabata, K. Takasan, S. Higashikawa, and M. Ueda, Topological phases of non-Hermitian systems, Phys. Rev. X **8**, 031079 (2018).
- [143] K. Kawabata, S. Higashikawa, Z. Gong, Y. Ashida, and M. Ueda, Topological unification of time-reversal and particle-hole symmetries in non-Hermitian physics, Nat. Commun. **10**, 297 (2019).
- [144] H. Zhou and J. Y. Lee, Periodic Table for Topological Bands with Non-Hermitian Bernard-LeClair Symmetries, arXiv:1812.10490.
- [145] K. Kawabata, K. Shiozaki, M. Ueda, and M. Sato, Symmetry and Topology in Non-Hermitian Physics, arXiv:1812.09133.
- [146] K. Kawabata, T. Bessho, and M. Sato, Non-Hermitian Topology of Exceptional Points, arXiv:1902.08479.
- [147] A. Szameit, M. C. Rechtsman, O. Bahat-Treidel, and M. Segev,  $\mathcal{PT}$ -symmetry in honeycomb photonic lattices, Phys. Rev. A **84**, 021806(R) (2011).
- [148] H. Zhou, C. Peng, Y. Yoon, C. W. Hsu, K. A. Nelson, L. Fu, J. D. Joannopoulos, M. Soljačić, and B. Zhen, Observation of bulk Fermi arc and polarization half charge from paired exceptional points, Science **359**, 1009 (2018).
- [149] S. Lin, L. Jin, and Z. Song, Symmetry protected topological phases characterized by isolated exceptional points, Phys. Rev. B **99**, 165148 (2019).
- [150] V. Kozii and L. Fu, Non-Hermitian Topological Theory of Finite-Lifetime Quasiparticles: Prediction of Bulk Fermi Arc Due to Exceptional Point, arXiv:1708.05841.
- [151] S. Malzard and H. Schomerus, Bulk and edge-state arcs in non-Hermitian coupled-resonator arrays, Phys. Rev.

- A **98**, 033807 (2018).
- [152] J. C. Budich, J. Carlström, F. K. Kunst, and E. J. Bergholtz, Symmetry-protected nodal phases in non-Hermitian systems, *Phys. Rev. B* **99**, 041406(R) (2019).
  - [153] R. Okugawa and T. Yokoyama, Topological exceptional surfaces in non-Hermitian systems with parity-time and parity-particle-hole symmetries, *Phys. Rev. B* **99**, 041202(R) (2019).
  - [154] A. Cerjan, M. Xiao, L. Yuan, and S. Fan, Effects of non-Hermitian perturbations on Weyl Hamiltonians with arbitrary topological charges, *Phys. Rev. B* **97**, 075128 (2018).
  - [155] H. Zhou, J. Y. Lee, S. Liu, and B. Zhen, Exceptional surfaces in  $\mathcal{PT}$ -symmetric non-Hermitian photonic systems, *Optica* **6**, 190 (2019).
  - [156] A. Cerjan, S. Huang, K. P. Chen, Y. Chong, and M. C. Rechtsman, Experimental realization of a Weyl exceptional ring, arXiv:1808.09541.
  - [157] T. Yoshida, R. Peters, N. Kawakami, and Y. Hatsugai, Symmetry-protected exceptional rings in two-dimensional correlated systems with chiral symmetry, *Phys. Rev. B* **99**, 121101(R) (2019).
  - [158] J. González and R. A. Molina, Topological protection from exceptional points in Weyl and nodal-line semimetals, *Phys. Rev. B* **96**, 045437 (2017); R. A. Molina and J. González, Surface and 3D quantum Hall effects from engineering of exceptional points in nodal-line semimetals, *Phys. Rev. Lett.* **120**, 146601 (2018).
  - [159] J. Carlström, M. Stålhammar, J. C. Budich, and E. J. Bergholtz, Knotted non-Hermitian metals, *Phys. Rev. B* **99**, 161115(R) (2019).
  - [160] Supplemental Materials for the vector field and the graphic eigenstates in the broken  $\mathcal{PT}$  phase.
  - [161] D. Leykam, M.C. Rechtsman, and Y.D. Chong, Anomalous Topological Phases and Unpaired Dirac Cones in Photonic Floquet Topological Insulators, *Phys. Rev. Lett.* **117**, 013902 (2016).
  - [162] M. Xiao, W. J. Chen, W. Y. He, and C. T. Chan, Synthetic gauge flux and Weyl points in acoustic systems, *Nat. Phys.* **11**, 920 (2015); Z. Yang, F. Gao, X. Shi, X. Lin, Z. Gao, Y. Chong, and B. Zhang, Topological Acoustics, *Phys. Rev. Lett.* **114**, 114301 (2015).
  - [163] R. Fleury, A. B. Khanikaev, and A. Alù, Floquet topological insulators for sound, *Nat. Commun.* **7**, 11744 (2016).
  - [164] C. He, X. Ni, H. Ge, X. C. Sun, Y. B. Chen, M. H. Lu, X. P. Liu and Y. F. Chen, Acoustic topological insulator and robust one-way sound transport, *Nat. Phys.* **12**, 1124 (2016).
  - [165] Y. Wang, L. J. Lang, C. H. Lee, B. Zhang, and Y. D. Chong, Topologically enhanced harmonic generation in a nonlinear transmission line metamaterial, *Nat. Commun.* **10**, 1102 (2019).
  - [166] C. H. Lee, S. Imhof, C. Berger, F. Bayer, J. Brehm, and L. W. Molenkamp, Tobias Kiessling and Ronny Thomale Topoelectrical Circuits, *Commun. Phys.* **1**, 39 (2018).
  - [167] M. Ezawa, Electric-circuit realization of Hermitian and non-Hermitian Majorana edge states, arXiv:1902.03716; Electric circuits for non-Hermitian Chern insulators, arXiv:1904.03823.

**SUPPLEMENTAL MATERIAL FOR “VISUALIZING TOPOLOGY OF REAL-ENERGY GAPLESS PHASE ARISING FROM EXCEPTIONAL POINT”**

X. M. Yang, P. Wang, L. Jin, and Z. Song

*School of Physics, Nankai University, Tianjin 300071, China*

**A: Vector field**

The core matrix in the momentum space reads  $h_k = \mathbf{B} \cdot \boldsymbol{\sigma} = B_x \sigma_x + B_y \sigma_y + B_z \sigma_z$ . We consider  $B_x$  and  $B_y$  are real, but  $B_z$  is imaginary, then the eigenstates of  $h_k$  within the range of real eigenvalues  $\varepsilon_k^\pm$  can be written in the form of Eq. (1) of the Letter, and the average values of Pauli matrices can be expressed as

$$\begin{aligned} \langle \sigma_x \rangle_\pm &= \langle \psi_k^\pm | \sigma_x | \psi_k^\pm \rangle = \cos(-\varphi_\pm) \\ \langle \sigma_y \rangle_\pm &= \langle \psi_k^\pm | \sigma_y | \psi_k^\pm \rangle = \sin(-\varphi_\pm) . \\ \langle \sigma_z \rangle_\pm &= \langle \psi_k^\pm | \sigma_z | \psi_k^\pm \rangle = 0 \end{aligned} \quad (10)$$

The average values of Pauli matrices define a vector field that related to the topological features of the non-Hermitian topological system. The vector field  $\mathbf{F}_\pm(k) = (\langle \sigma_x \rangle_\pm, \langle \sigma_y \rangle_\pm)$  directly relates to the phase factor  $\varphi_\pm$  of the eigenstates. For the non-Hermitian SSH ladder, the core matrix is in Eq. (6) of the Letter. Within the range of real eigenvalues  $\varepsilon_k^\pm$ , the corresponding eigenstates of  $h_k$  in Eq. (1) of the Letter have  $\varphi_+ = \theta_1 + \theta_2$  and  $\varphi_- = \theta_1 - \theta_2 \pm \pi$ , and  $\tan \theta_1 = [(w - v) \sin k] / [(v + w) \cos k]$ ,  $\tan \theta_2 = \gamma / (|we^{-ik} + ve^{ik} + t|^2 - \gamma^2)^{1/2}$ . The complete information of graphic eigenstates are mapped to the phases  $\varphi_\pm(k)$ .

**B: Graphic eigenstates in the broken phase**

Under the periodical boundary condition of the non-Hermitian SSH ladder, the effective complex magnetic field is  $B_x = (v + w) \cos k + t$ ,  $B_y = (v - w) \sin k$ , and  $B_z = i\gamma$  in the core matrix  $h_k$ . For large non-Hermiticity  $\gamma > \gamma_c$  in the broken parity-time phase, the complex energy levels appear; and the corresponding eigenstates of  $h_k$  reduce to the form of

$$|\psi_k^\pm\rangle = \begin{pmatrix} \sin(\theta_\pm/2)e^{i\varphi_\pm} \\ \cos(\theta_\pm/2) \end{pmatrix}. \quad (11)$$

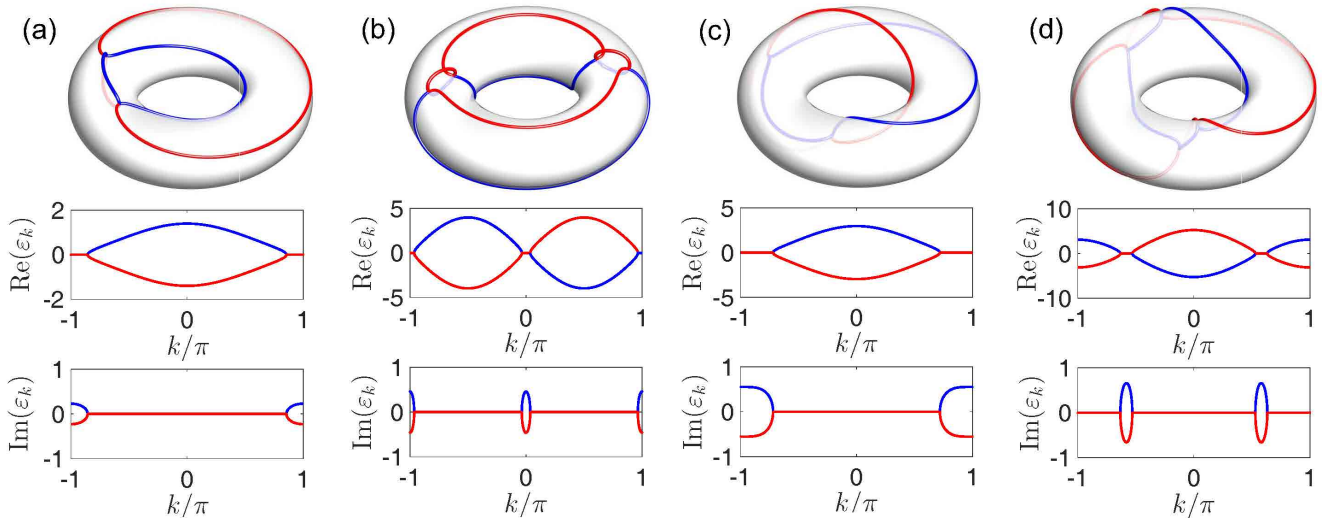


FIG. 4. Graphic eigenstates and energy bands in the broken  $\mathcal{PT}$ -symmetric phase of the non-Hermitian SSH ladder.  $(v, w, \gamma)$  is (a)  $(1/4, 1/4, 11/20)$ , (b)  $(-2, 2, 11/10)$ , (c)  $(2, 2/7, 7/5)$ , (d)  $(3, 3/2, 8/5)$ . In all plots,  $t = 1$ .

For the complex  $\varepsilon_k$ ,  $\varphi_+ = \varphi_- = \arctan(-B_y/B_x)$  and  $\theta_{\pm} = 2 \arccos(1/\sqrt{C_{\pm}})$  where  $C_{\pm} = |B_z \pm B|^2 / (B_x^2 + B_y^2) + 1$  is the normalization coefficient. In the  $\varphi$ - $k$  torus,  $R_0$  is the distance from the center of the tube to the center of the torus, and  $r_0$  is the radius of the tube. Two loops are plotted on the torus with  $R = R_0$  and  $r = r_0 + \cos\theta_{\pm}$ . We have  $\theta_{\pm} = \pi/2$  for the real-energy levels, thus the real-energy levels of the two loops are always located on the surface ( $r = r_0$ ) of the  $\varphi$ - $k$  torus, while the complex energy levels of the two loops are shifted to outside ( $r > r_0$ ) or inside ( $r < r_0$ ) the surface of the  $\varphi$ - $k$  torus. The graphic eigenstates and energy bands of the non-Hermitian SSH ladder in the broken parity-time symmetric phase are depicted in Supplemental Figures 4(a)-(d) as a comparison with those in the real-energy gapless phase arising from exceptional points shown in Figs. 1(e)-1(h) of the Letter.